Correction

DEVELOPMENTAL BIOLOGY

Correction for "*Drosophila* E-cadherin is required for the maintenance of ring canals anchoring to mechanically withstand tissue growth," by Nicolas Loyer, Irina Kolotuev, Mathieu Pinot, and Roland Le Borgne, which was first published September 30, 2015; 10.1073/pnas.1504455112 (*Proc Natl Acad Sci USA* 112:12717–12722).

The authors note that Fig. 6 and its corresponding legend appeared incorrectly. The corrected figure and its corrected legend appear below.

The authors also note that on page 12720, right column, first paragraph, line 7, "the E-Cad^{+} clusters" should instead appear as "the E-Cad/β-Cat clusters"; on page 12721, right column, fourth full paragraph, line 4, "1:100; DSHB" should instead appear as "1:100: BD Biosciences"; and, in the same paragraph, line 5, "1:50; DSHB" should instead appear as "1:50; ab50599; AbCam."

The authors also note that, in the Supporting Information, page 1, right column, first full paragraph, line 19, "E-Cad clusters" should instead appear as "E-Cad/β-Cat clusters"; on the same page, right column, second full paragraph, lines 2–3, "1:100; DSHB" should instead appear as "1:100; BD Biosciences"; and, in the same paragraph, line 4, "1:50; DSHB" should instead appear as "1:50; ab50599; AbCam." The SI has been corrected online.

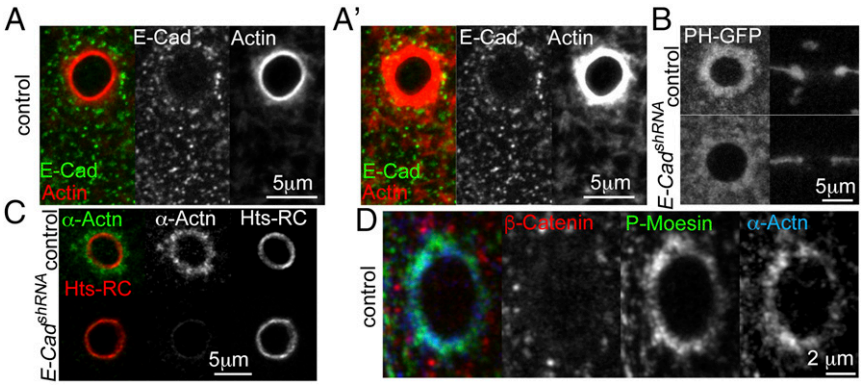

Fig. 6. E-Cad organizes microvillosity-like structures. (*A* and *A′*) RC from a control stage 8 fixed GC stained for E-Cad (green) and actin (red). Actin staining is displayed under two different brightness/contrast settings to illustrate properly both the faint actin-positive filaments all over the cortex (seen better in *A′*) and the intense actin signal at the periphery of RCs (seen better in *A*). (*B*) RCs from control and E-Cad *shRNA*^{GL00646} live stage 8 GCs expressing the PH::GFP probe. (*C*) Control and E-Cad *shRNA*^{GL00646} fixed stage 8 GCs stained for Actn (green) and the inner rim marker Hts-RC (red). (*D*) Control fixed stage 9 GC stained for β-Cat (red), P-Moesin (green), and Actn (blue). Adhesive clusters are more peripheral than the portion of P-Moesin/Actn^{+} PM surrounding the RCs.

Published online September 17, 2018.

www.pnas.org/cgi/doi/10.1073/pnas.1814899115

Drosophila E-cadherin is required for the maintenance of ring canals anchoring to mechanically withstand tissue growth

Nicolas Loyer[a,b,c,1], Irina Kolotuev[a,b,c,d], Mathieu Pinot[a,b,c], and Roland Le Borgne[a,b,c,2]

[a]CNRS, UMR 6290, F-35000 Rennes, France; [b]Institut de Génétique et Développement de Rennes, Université Rennes 1, F-35000 Rennes, France; [c]Equipe Labellisée Ligue Nationale Contre le Cancer, F-35000 Rennes, France; and [d]CNRS, Structure Fédérative de Recherche BIOSIT, Microscopy Rennes Imaging Center-Electron Microscopy Facility, F-35000 Rennes, France

Edited by Jean-Rene Huynh, Institut Curie, Paris, France, and accepted by the Editorial Board September 9, 2015 (received for review March 19, 2015)

Intercellular bridges called "ring canals" (RCs) resulting from incomplete cytokinesis play an essential role in intercellular communication in somatic and germinal tissues. During *Drosophila* oogenesis, RCs connect the maturing oocyte to nurse cells supporting its growth. Despite numerous genetic screens aimed at identifying genes involved in RC biogenesis and maturation, how RCs anchor to the plasma membrane (PM) throughout development remains unexplained. In this study, we report that the clathrin adaptor protein 1 (AP-1) complex, although dispensable for the biogenesis of RCs, is required for the maintenance of the anchorage of RCs to the PM to withstand the increased membrane tension associated with the exponential tissue growth at the onset of vitellogenesis. Here we unravel the mechanisms by which AP-1 enables the maintenance of RCs' anchoring to the PM during size expansion. We show that AP-1 regulates the localization of the intercellular adhesion molecule E-cadherin and that loss of AP-1 causes the disappearance of the E-cadherin–containing adhesive clusters surrounding the RCs. E-cadherin itself is shown to be required for the maintenance of the RCs' anchorage, a function previously unrecognized because of functional compensation by N-cadherin. Scanning block-face EM combined with transmission EM analyses reveals the presence of interdigitated, actin- and Moesin-positive, microvilli-like structures wrapping the RCs. Thus, by modulating E-cadherin trafficking, we show that the sustained E-cadherin–dependent adhesion organizes the microvilli meshwork and ensures the proper attachment of RCs to the PM, thereby counteracting the increasing membrane tension induced by exponential tissue growth.

E-cadherin | membrane tension | tissue growth | ring canals | trafficking

E-cadherin (E-Cad) is a core component of intercellular adhesion complexes in cohesive metazoan tissues. E-Cad assembles into clusters that are stabilized by actin filaments via β- and α-catenin at the level of adherens junctions and form an adhesive belt mechanically linking cells together. A key feature of adherens junctions is their plasticity, which enables tissue remodeling, sustained by a constant endocytosis- and exocytosis-regulated E-Cad turnover (1) that is critical for various morphogenetic processes in epithelia (2–5).

Drosophila oogenesis is a rich, multifaceted developmental process during which E-Cad function is not limited to epithelia, because it also regulates intercellular collective migration (6, 7) and the adhesion of stem cells to their niche (8). Cells derived from two different stem cell populations initially assemble into egg chambers composed of a follicular epithelium surrounding a 16-cell germline cyst (GC), itself composed of one oocyte and 15 nurse cells. During the next 64 h, GC cells grow to hundreds of times their initial volume. Oocyte growth is supported by cytoplasmic connections with nurse cells through ring canals (RCs) (Fig. 1 *A* and *B*), intercellular bridges that, instead of undergoing abscission, are stabilized on arrested cleavage furrows (9, 10). Recent findings revealed that RCs play a vital role in germline as well as in somatic tissues (10). RCs are composed of a noncontracting subcortical actin ring (11), the inner rim, attached to an electron-dense plasma membrane (PM) (12), the outer rim (Fig. 1*A*). RCs have been studied mainly in *Drosophila* female GCs (9) where genetic screens uncovered a variety of actin regulators controlling their establishment at the onset of oogenesis and their growth throughout the entire process (13–17). However, the molecular machinery involved in anchoring the PM to the RC remains unknown. Mutations in several membrane-traffic regulators affect the integrity of nurse cells' PM, causing multinucleation and giving rise to remnants of detached RCs (18–24); these observations suggest that an unidentified membrane cargo is required for anchoring RCs to the PM.

Here we describe an RC detachment phenotype in mutants of the clathrin adaptor protein 1 (AP-1), a protein complex regulating polarized membrane protein sorting from the *trans*-Golgi network and endosomal compartments (25), and provide direct evidence that polarized membrane trafficking to RCs allows an E-Cad–mediated mechanical strengthening of RC anchoring necessary to resist the membrane tension generated by cellular growth.

Results

Loss of AP-1 Induces Multinucleation of Nurse Cells in Female GCs. In this study we generated homozygous *AP-47^{SHE11}* mutant GCs in the female germline (the μ subunit of AP-1, hereafter referred to as "*AP-1* mutants"). Actin staining revealed that nurse cells of *AP-1*

Significance

This work addresses the interplay among membrane trafficking, cell adhesion, and tissue integrity maintenance in the *Drosophila* female germline. The clathrin adaptor protein 1 (AP-1) complex is shown to regulate the trafficking of E-cadherin to ring canals (RCs), a structure resulting from incomplete cytokinesis and allowing intercellular communication. E-cadherin assembles adhesive clusters that, as revealed by EM analyses, organize a dense microvilli meshwork wrapping around RCs. Although dispensable for RC biogenesis and maturation, AP-1 and E-cadherin are required to maintain RCs' anchoring to the plasma membrane at the onset of vitellogenesis, when cells experience exponential growth and increased mechanical stress. Our study unravels a previously unidentified function for E-cadherin in maintaining RC anchoring to the plasma membrane.

Author contributions: N.L. and R.L.B. designed research; N.L., I.K., and M.P. performed research; N.L. contributed new reagents/analytic tools; N.L., I.K., M.P., and R.L.B. analyzed data; and N.L. and R.L.B. wrote the paper.

The authors declare no conflict of interest.

This article is a PNAS Direct Submission. J.-R.H. is a guest editor invited by the Editorial Board.

[1]Present address: College of Life Sciences, University of Dundee, Dundee DD15EH, Scotland, United Kingdom.

[2]To whom correspondence should be addressed. Email: roland.leborgne@univ-rennes1.fr.

This article contains supporting information online at www.pnas.org/lookup/suppl/doi:10.1073/pnas.1504455112/-/DCSupplemental.

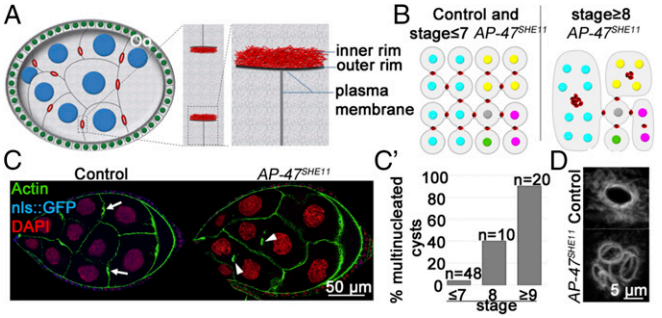

Fig. 1. Nurse cells' multinucleation in AP-1 mutant female GCs. (*A*) Schematic representation of the GC consisting of a single oocyte (Oo, nucleus) connected to 15 nurse cells (blue) via RCs (red) and a surrounding monolayer of about 650 somatic follicle cells (green). (*Inset*) Schematic representation of a transverse section through the RCs composed of an inner rim [red, containing the Adducin-like Hu-li tai shao (Hts) (13, 15) and the filamin Cheerio (16)] contacting an electron-dense PM (outer rim, black) that itself is connected to the rest of the nurse cell PM (gray). (*B*) Stereotyped organization of the female GC before and after detachment of nurse cells' RCs. The oocyte has a gray nucleus; nurse cells have colored nuclei. (*C*) Stage 8 wild-type and *AP-1* mutant [identified by the loss of nuclear localization signal (NLS)::GFP, blue] GCs stained for actin (green) and DAPI (red). Arrows indicate RCs connecting nurse cells in control GCs. Arrowheads indicate RCs floating in the cytoplasm of multinucleated nurse cells in *AP-1* mutant GCs (at least one floating ring was observed in 29 of 34 mutant stage 8 or older GCs). (*C'*) Quantitation of multinucleated *AP-1* mutant GCs at stage 7 to stage 9 or older. (*D*) Maximal projections of 5 µm of anchored and clustered floating RCs in control and *AP-1* mutant GCs.

mutant GCs progressively became multinucleated, exhibiting floating RCs organized in clusters (Fig. 1 *C* and *D*). Multinucleation, indicating a defect in membrane stability, was first observed at the onset of vitellogenesis (stage 8). Loss of AP-1 never caused loss of oocyte membrane integrity, suggesting that this membrane is more robust than that of nurse cells, presumably because of its differential organization and composition (26).

A Faster Growth Rate Correlates with Higher PM Tension. Multinucleation begins at a stage during which the oocyte accumulates yolk and GCs grow 4.6 (stage 8) to 34 (stage 10a) times faster than at previous stages (Fig. 2 *A* and *B*). Because a faster growth rate could affect mechanical membrane properties, providing a rational for this stage-dependent multinucleation phenotype, we probed PM tension by making 5-µm-wide holes in nurse cells' PM using laser ablation. Such holes did not heal but instead propagated until they reached the PM of neighboring nurse cells, leading to multinucleation (Fig. 2*C* and Movie S1). We measured the retraction of PM extremities and vertices after ablation and found that membrane recoil was about four times slower (1 µm/min) than in epidermal cells and did not differ significantly in slow- and fast-growing GCs (Fig. 2*D* and Fig. S1 *B–E*). However, cutting the sheet-like nurse cell–nurse cell interface may not release tension as efficiently as cutting the string-like belt of adherens junctions in epithelia. Furthermore, tensions may not be released as efficiently at later stages as at the earlier ones, because we made holes of the same size in nurse cell–nurse cell interfaces although the surfaces of these interfaces differ by 4.5-fold between stages 5 and 9.

Although these two experimental biases prevented us from assessing PM tension directly, we noticed that adjacent nurse cells were subjected to more fluctuations in cell shape when ablation was performed at early stages rather than later stages (Fig. S1 *A* and *A'*). This observation indicates that PMs are more prone to deformations at early stages, possibly because of lower PM tension. Accordingly, we observed that after ablation, tubular pleckstrin homology domain::GFP^{+} (PH::GFP^{+}) deformations appeared on the PM contacting adjacent nurse cells (Fig. 2*E*, arrowheads). Because such tubular deformations are reminiscent of those observed in vitro at the surface of giant unilamellar vesicles and in vivo at the PM of cells upon the reduction of PM tension (27, 28), we reasoned that tension release induced by ablation is causal to the appearance of deformations. We found that tubular deformations were frequent in slow-growing GCs but were hardly detectable in fast-growing ones (Fig. 2 *E* and *F*, Fig. S1*H*, and Movies S2 and S3). Strikingly, PM tubular deformations already were present before ablation in slow-growing GCs but not in fast-growing ones (Fig. 2 *E* and *F*) and therefore (because their presence does not rely on laser ablation) could be used as a reliable readout for PM tension. Thus, we concluded that the PM tension is higher in stages 8–10a GCs than at earlier stages. Finally, similar recoil velocities and tubular deformations following laser ablation were obtained upon loss of AP-1, indicating that AP-1 does not significantly regulate PM tension (Fig. S1 *F–H*). PM tension is the sum of the in-plane lipid bilayer tension and the protein-dependent membrane-to-cortex attachment (29). We did not further assess the respective contributions of these factors to changes in PM tension during oogenesis, but we propose that the exponential growth that begins at stage 8 affects the mechanical membrane properties, eventually causing multinucleation in *AP-1* mutants.

AP-1 and Rab11 Control the Maintenance of RC Anchoring to the PM and E-Cad Localization in Nurse Cells. To follow the dynamics of the disappearance of the PM, we monitored the distribution of the PM marker E-Cad using an E-Cad::GFP knockin line (30) in *AP-1* mutant GCs. Live imaging revealed that multinucleation was caused by the detachment of the PM from RCs, immediately followed by PM fragmentation (Fig. 3*A*). We never observed fragmentation of portions of PM devoid of RCs, suggesting that multinucleation was caused exclusively by the detachment of the PM from the RCs. This notion was supported further by our analysis of fixed tissue: According to the stereotyped organization of the GC, loss of all RCs connecting nurse cells to nurse cells but not of RCs connecting nurse cells to the oocyte should lead to the formation of three syncytia containing two, four, and eight

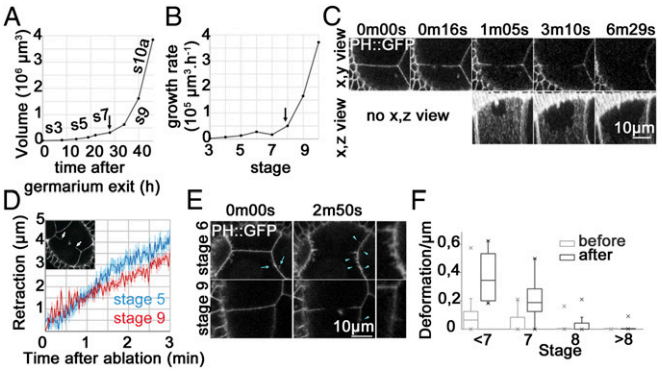

Fig. 2. A faster growth rate correlates with an increase in PM tension. (*A*) The change in GC volume after exit from the germarium. Oogenesis stages are indicated above the curve. The arrow indicates the onset of vitellogenesis. (*B*) GC growth rates from stages 3–10a. The arrow indicates the onset of vitellogenesis. (*C*) Nano-ablation of a PM from the nurse cell of a stage 7 GC expressing PH::GFP. The PM regresses progressively after a 5-µm-long wound was made. (*Upper*) Confocal planes where the wound was made. (*Lower*) Orthogonal views to visualize the entire targeted portion of the PM. (*D*) Displacement of the free PM extremities (arrows in the *Inset*) generated by PM laser ablation in stage 5 and stage 9 nurse cells. (*E*) Representative cases of ablation of nurse cells' PM from stage 6 (*Upper*) and stage 9 (*Lower*) GCs. PM deformations were observed before the cut (arrows) in stage 6 GCs but not in stage 9 GCs, and more deformations appear after the cut in the PM contiguous to ablated PM (arrowheads) in stage 6 GCs than in stage 9 GCs. (*F*) Density of deformations in the PM contiguous to the ablated PM before and after the cut (stages 5 and 6, $n = 14$; stage 7, $n = 26$; stage 8, $n = 23$; and stages 9 and 10, $n = 23$).

nurse cell nuclei. This exact configuration was observed in *AP-1* mutants (Figs. 1*B* and 3*B*), further indicating that nurse cell–nurse cell interfaces devoid of RCs remain stable in the AP-1 mutant and that nurse cells' multinucleation is caused by RC detachment. Thus, although dispensable for RC establishment, AP-1 activity is required to maintain RCs' anchoring to the PM beginning at stage 8.

Live imaging of E-Cad::GFP and immunostaining of endogenous untagged E-Cad revealed that the whole surface of nurse cells' PM is decorated by E-Cad^{+} clusters visibly enriched around RCs (Fig. 3*C*). In *AP-1* mutant GCs, this enrichment started to disappear at stage 8 (Fig. 3 *C* and *C′*). In mutant GCs, E-Cad also localized to cytoplasmic puncta that were absent from control cells and already were present in non-multinucleated GCs at stage 8 (Fig. 3*E*), indicating that cytoplasmic mislocalization of E-Cad in *AP-1* mutant GCs precedes multinucleation. In mammalian cells, AP-1 controls the subcellular localization and function of the Rab11^{+} recycling endosome compartment (31, 32), and E-Cad transits through Rab11^{+} compartments (33–35). This function raises the possibility that E-Cad mislocalization in *AP-1* mutants involves a defect in Rab11-dependent trafficking. Consistent with this proposition, Rab11 localization changed from small endosomes distributed throughout the entire cytoplasm in control nurse cells to enlarged endosomes in *AP-1* mutant nurse cells (Fig. 3*D*), and the majority of E-Cad cytoplasmic puncta localized to Rab11^{+} compartments (Fig. 3*E*). To assess the effect of Rab11 on E-Cad trafficking, we overexpressed a dominant-negative form of Rab11 (Rab11^{S25N}) that was reported to block entry into recycling endosomes in mammalian cells (36). Overexpression of Rab11^{S25N} phenocopied *AP-1* mutants with loss of E-Cad enrichment around RCs (Fig. 3*F*) and multinucleation of stage 8 and older nurse cells (Fig. 3*G*). Thus, in both *AP-1* and *Rab11* mutant backgrounds, the presence of fewer E-Cad clusters surrounding RCs correlates with RC detachment leading to multinucleation.

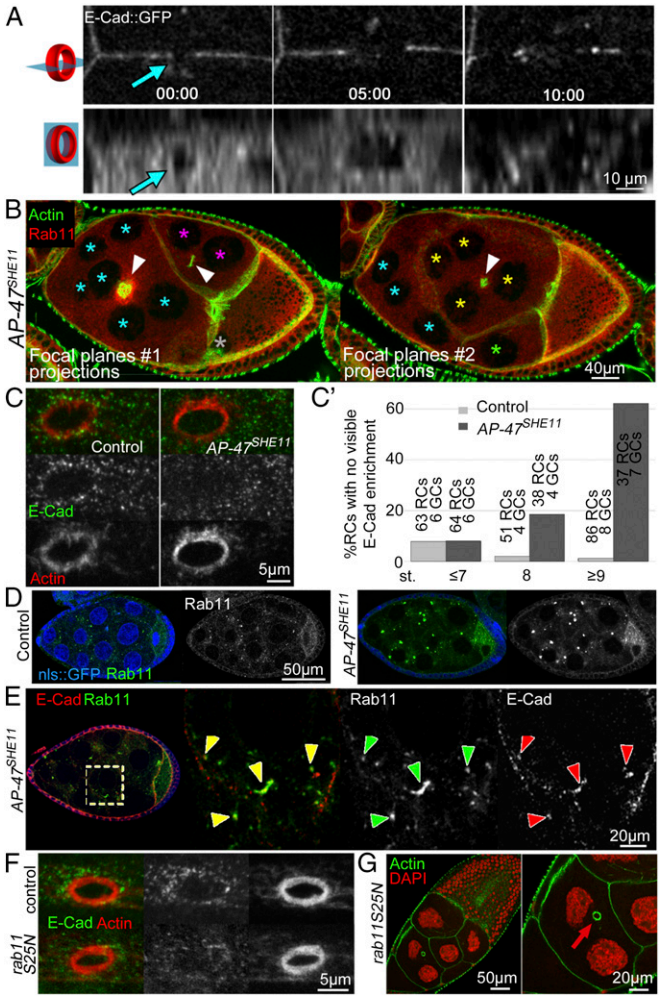

Fig. 3. AP-1 and Rab11 control the maintenance of RCs' anchoring and E-Cad localization in nurse cells. (*A*) Time-lapse imaging of a stage 8 *AP-1* mutant GC. The RC is seen as a hole (arrow) in the otherwise continuous E-Cad::GFP^{+} PM. (*Upper*) Single focal planes. (*Lower*) Orthogonal sections. PM detachment starting from the RC (t = 5 s) is followed by PM fragmentation (t = 10 s, n = 5). (*B*) A stage 9 *AP-1* mutant GC stained for actin (green) and Rab11 (red). The two panels correspond to projections of different focal planes. With the exception of the oocyte (gray asterisk), every nurse cell PM initially bearing an RC collapsed, resulting in three syncytia containing 8, 4, and 2 nurse cell nuclei (as indicated by colored asterisks and the corresponding cartoon in Fig. 1*B*) and clusters of detached RCs (arrowheads). (*C*) RCs in stage 9 GCs stained for E-Cad (green) and actin (red) (maximal projections of 5–7 µm). E-Cad is enriched around RCs, and this enrichment can be lost in stage 8 and older *AP-1* mutants. (*C′*) Quantification of data in *C*. Total numbers of RCs and GCs examined are indicated above the columns. (*D*) Stage 8 control (NLS::GFP^{+}) and *AP-1* mutant (NLS::GFP^{-}) GCs stained for Rab11. Enlarged endosomes were observed in 17 of 18 *AP-1* mutant GCs (from stages 4–10). (*E*) Stage 8 *AP-1* mutant nurse cell stained for E-Cad and Rab11. An entire GC is shown at low magnification in the left panel. The other three panels show magnified views of the boxed area in the left panel. Arrowheads indicate enlarged endosomes positive for Rab11 and E-Cad, which partially colocalized in 12 of 16 stage 4–10 GCs. In three stage 8 GCs, 94% of E-Cad^{+} endosomes (145/155) were positive for Rab11, and 63% of Rab11^{+} endosomes (145/222) were positive for E-Cad. (*F*) RCs of stage 9 GCs overexpressing WT Rab11 or Rab11^{S25N} were stained for E-Cad (green) and actin (red) (maximal projections of 5–7 µm). Loss of E-Cad enrichment was seen in 35 of 83 RCs from 10 stage 9 or older Rab11^{S25N}-expressing GCs. (*G*) A stage 10 GC overexpressing Rab11^{S25N}. The arrow indicates floating RCs (seen in 9 of 13 stage 8 or older GCs). The right panel shows a magnified view of the boxed area in the left panel.

E-Cad Controls RCs Anchoring to the PM. This correlation raises the possibility that E-Cad/Shotgun (Shg) is necessary to anchor RCs. Consistent with this suggestion, GCs mutant for the *shg^{IG29}* loss-of-function allele (37) and null β-catenin (β-Cat) alleles *arm^{XP33}* (Fig. 4*A*), *arm^{YD35}*, or *arm^{XK22}* (6, 37, 38) display nurse cell multinucleation. However, the amorphic *shg^{IH}* and the null *shg^{R69}* mutant alleles do not cause nurse cell multinucleation (6, 39). We reasoned that this apparent discrepancy could be explained by functional compensation by the classical cadherin N-cadherin (N-Cad) in E-Cad–null mutant GCs, as reported in other tissues in ref. 40. We found that N-Cad was not detected in control GCs, but in *E-Cad*-null mutant GCs N-Cad was expressed ectopically and was localized to the PM (Fig. 4*B*). We propose that E-Cad somehow negatively regulates N-Cad transcription and/or translation, although we cannot rule out the possibility that N-Cad is translated in control GCs but is targeted to degradation and is below our detection threshold. Nevertheless, in the absence of E-Cad, β-Cat still localized to the PM of nurse cells, albeit at lower levels than in controls (Fig. 4*B*), as is consistent with functional compensation. This observation prompted us to prevent N-Cad ectopic expression by using *N-Cad^{RNAi}* in *E-Cad*–null mutant GCs. N-Cad silencing in *shg^{+}* GCs did not cause any detectable phenotype (n = 30), but N-Cad silencing in *shg^{R69}* mutant GCs induced multinucleation (Fig. 4*C*) in addition to the oocyte mispositioning defects expected from the loss of E-Cad (39). Furthermore, we observed that *shRNA*-mediated E-Cad depletion also caused nurse cell multinucleation (Fig. 4*D*). In this situation, we speculate that incomplete E-Cad depletion is sufficient to disrupt E-Cad function in RC anchoring but not in repressing N-Cad expression. Accordingly, N-Cad was not ectopically expressed, and β-Cat was no longer recruited to the PM in E-Cad–depleted GCs (Fig. S2). Together, our results show that N-Cad is responsible for a functional compensation of E-Cad loss in RC anchoring, explaining why nurse cell multinucleation is observed in β-Cat– but not in E-Cad–null alleles, and enable us to conclude that E-Cad participates in RCs anchoring.

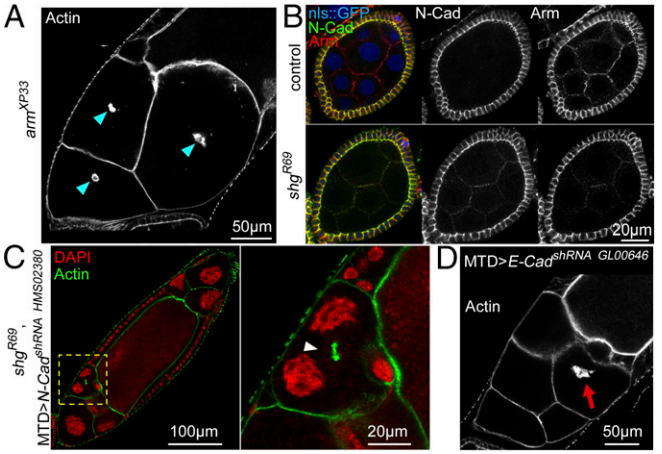

Fig. 4. E-Cad controls RCs' anchoring to the PM. (*A*) Stage 10 *arm* mutant GCs stained for Actin. Arrowheads indicate floating RCs (at least one floating RC was seen in three of four arm^{XP33} mutant stage 8 or older GCs). (*B*) Stage 6 control and E-Cad mutant (shg^{R69}) GCs stained for N-Cad (green) and Armadillo (red). Ectopic expression of N-Cad was observed in 15 of 15 stage 4 and older shg^{R69} GCs. (*C*) A stage 10 E-Cad mutant GC expressing N-Cad $shRNA^{HMS02380}$ stained for DAPI (red) and actin (green). Floating RCs (arrowhead) were observed in 5 of 10 stage 8 or older GCs. The right panel shows a magnified view of the boxed area in the left panel. (*D*) GCs expressing E-Cad $shRNA^{GL00646}$ in stage10 egg chambers stained for actin. The arrow indicates floating a RC. (At least one floating RC was seen in 14 of 22 E-Cad $shRNA^{GL00646}$ and in 10 of 13 E-Cad $shRNA^{HMS00693}$ stage 8 or older GCs.)

Disruption of a Microvillosities-Rich PM Around RCs in *AP-1* Mutant GCs. How exactly could the cadherin–catenin complex participate in the maintenance of RC anchorage? Transmission electron microscopy (TEM) analysis of multinucleated *AP-1* mutant GCs revealed that the inner rim of detached RCs remained attached to the outer rim, which itself was still connected to portions of the PM surrounding the RC (Fig. 5*A*). Thus, RC detachment does not result from the detachment of the inner rim from the outer rim but rather from the disconnection of a portion of the PM surrounding RCs. TEM further revealed that in control GCs the PM surrounding RCs appeared highly convoluted (Fig. 5 *A*–*B*′). In striking contrast, this region appeared devoid of such convolutions in RCs still anchored in *AP-1* mutant GCs, (Fig. 5 *B* and *B*′). We further examined the ultrastructural topology of the nurse cells' PMs using scanning block-face EM (41). This analysis shows that the complex convolutions surrounding RCs are caused by tightly packed tubular extensions of PM, 65 ± 14 nm in diameter and 1,500 ± 400 nm in length, that protrude into the intercellular space between nurse cells (Fig. 5*C* and Movies S4 and S5). Such protrusions also were observed at lower density over the rest of the PM distant from RCs (Fig. 5 *C* and *D* and Movies S4 and S5). We further characterized these structures using light microscopy. We propose that actin-positive filaments at the PM at a distance from RCs (Fig. 6*A*) correspond to individual protrusions and that the high density of actin (Fig. 6*A*) and the presence of the actin crosslinker α-Actinin (Actn) (Fig. 6 *C* and *D*) (42), the actin regulator Enabled (43), and the microvilli marker phospho-Moesin (Fig. 6*D*) at the PM surrounding RCs is caused by the local abundance of the protrusions revealed by TEM (Fig. 5*A*). *AP-1* mutant cells displayed lower levels of Actn around RCs (Fig. S3*A*), consistent with the loss of PM convolutions around RCs (Fig. 5 *B* and *B*′), further indicating that AP-1 is necessary for protrusions organization around RCs.

E-Cad Organizes Microvillosity-Like Structures in Nurse Cells. Loss of E-Cad enrichment and loss of protrusions around RCs in *AP-1* mutants prompted us to analyze the direct requirement for E-Cad in protrusion organization. In E-Cad–depleted GCs, lower PH::GFP signals (Fig. 6*B*) and an almost complete loss of Actn signals around RCs indicate that protrusions surrounding RCs are severely affected (Fig. 6*C*). Furthermore, protrusions distributed all over the PM of nurse cells were visibly affected (Fig. S4 *A* and *A*′). Although this effect indicates that E-Cad controls the organization of protrusions, the $E\text{-}Cad^{+}$ clusters enriched around RCs do not localize to the protrusion-dense region but rather to its immediate periphery (Fig. 6 *A* and *D*), and clusters distributed all over the rest of the PM do not colocalize with actin-positive linear structures (Fig. 6*A*). Finally, we found that the polarity markers Par-3 and Discs large 1 (Dlg) that are enriched around RCs (Fig. S3*B*) also localized to the rest of the nurse cells' PM, but neither localized to microvilli (Fig. S3 *C* and *D*). Thus, we propose that AP-1–dependent E-Cad clusters organize protrusions independently of a polarized distribution of Par3 and Dlg.

Discussion

In this article, we report that AP-1/Rab11 regulate the polarized trafficking of E-Cad and that E-Cad assembles adhesive clusters that are needed to maintain the anchoring of RCs to the PM at the time of exponential GC growth; this growth is associated with a change in mechanical membrane properties that probably is caused by increased membrane tension.

We show that in *Drosophila* nurse cells, defects in AP-1/Rab11 function lead to the progressive disappearance of $E\text{-}Cad^{+}$ clusters

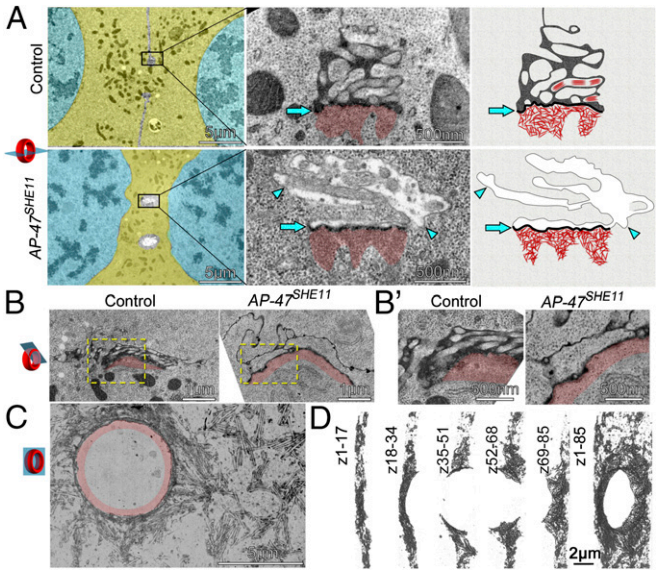

Fig. 5. Disruption of a microvillosity-rich PM around RCs in *AP-1* mutant GCs. (*A*) TEM image of anchored and detached RCs in control and *AP-1* mutant stage 9 GCs. (*Left*) Low magnifications; nuclei are cyan; cytosol is yellow. (*Center*) High-magnification views of the boxed areas in left panels. The RC actin-rich inner rim is red. (*Right*) Interpretative drawings of the center panels. The inner rim and parallel fibers inside protrusions are red. The inner rim (red) is attached to the outer rim (arrows, thick line) in anchored and detached RCs. The outer rim of the detached RC is itself still connected to a portion of PM (arrowheads). (*B* and *B*′) TEM image of control and *AP-1* mutant anchored RCs (stage 8). Boxed areas in *B* show a portion of the PM surrounding RCs. High magnifications of these areas in *B*′ show complex PM convolutions in the control and the absence of such convolutions in the mutant. (*C*) Projection over 3 μm (30 sections) of consecutive scanning block-face EM images of an RC (inner rim in red) and the neighboring PM in a control stage 8 GC. The RC is surrounded by microvilli-like protrusions also present at lower densities over the rest of the PM. (*D*) Consecutive projections over 1.7 μm (17 sections) of TEM images after PM segmentation through the volume of a RC in a control stage 8 GC and over 8.5 μm (85 sections) through its whole volume.

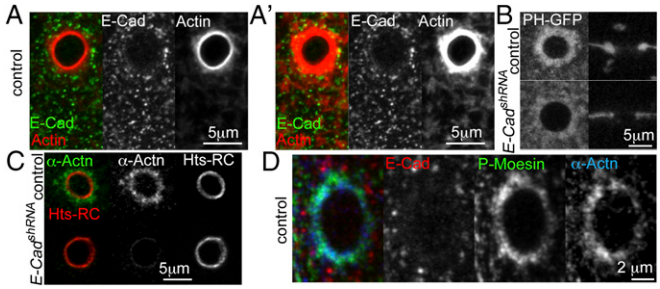

Fig. 6. E-Cad organizes microvillosity-like structures. (*A* and *A′*) RC from a control stage 8 fixed GC stained for E-Cad (green) and actin (red). Actin staining is displayed under two different brightness/contrast settings to illustrate properly both the faint actin-positive filaments all over the cortex (seen better in *A′*) and the intense actin signal at the periphery of RCs (seen better in *A*). (*B*) RCs from control and E-Cad *shRNA*^{GL00646} live stage 8 GCs expressing the PH::GFP probe. (*C*) Control and E-Cad *shRNA*^{GL00646} fixed stage 8 GCs stained for Actn (green) and the inner rim marker Hts-RC (red). (*D*) Control fixed stage 9 GC stained for E-Cad (red), P-Moesin (green), and Actn (blue). E-Cad clusters are more peripheral than the portion of P-Moesin/Actn^{+} PM surrounding the RCs.

surrounding RCs, suggesting that AP-1/Rab11 ensure the polarized delivery of E-Cad to RCs. Several studies in *Drosophila, Caenorhabditis elegans*, and mammals have implicated AP-1/Rab11 in E-Cad trafficking (33–35, 44, 45). Mammalian E-Cad carries a tyrosine-based AP-1 sorting signal, but the absence of such a motif in *Drosophila* E-Cad argues against a direct recognition of E-Cad by AP-1. Instead, interactions between E-Cad and membrane-trafficking regulators can be mediated by adaptors such as β-Cat (46) and the type I γ phosphatidylinositol phosphate kinase PIPKIγ (34). Alternatively, because AP-1 also controls the position and morphology of recycling endosomes (31, 32), the E-Cad trafficking defect we describe could result from malfunctioning recycling endosomes. Nurse cells' multinucleation also has been described for *Rab6* (18), *Rab11* (24), *PI4KIIIa* (23), and components of the Exocyst (20, 21) and ESCRT (19) complexes. Although the involvement of PI4KIIIa and ESCRT in E-Cad trafficking is unknown, E-Cad trafficking requires the activity of Rab6, Rab11, and the exocyst complex (46, 47). We therefore anticipate that defective intracellular trafficking of E-Cad toward adhesive clusters contributes to the multinucleation phenotypes in these trafficking regulators.

Whether AP-1 acts directly or not, this study unravels previously unidentified E-Cad functions. We show that E-Cad is required for the maintenance of RCs' anchorage. Intriguingly, E-Cad also organizes microvillosities at the surface of nurse cells, even though it does not localize to these microvillosities but rather to adhesive clusters interspersed between them. How could E-Cad organize microvilli remotely? One could speculate that close apposition of membranes through E-Cad–dependent adhesion somehow stabilizes protrusions, possibly by allowing specific contacts between protrusions. In epithelia, intermicrovillar adhesion is assured by protocadherins (48–50), and although any requirement for microvilli remains to be demonstrated, we envisage that they reinforce RCs anchorage. This remote action of E-Cad is somewhat reminiscent of another E-Cad function during oogenesis: E-Cad clusters at the nurse cells' PM control the orientation of the filopodia-like actin cables that position nuclei during later stages of oogenesis. In a similar fashion, these E-Cad clusters are interspersed between the membrane-originating tips of filopodia (51).

E-Cad functions in cell adhesion, migration, and stem cell maintenance during *Drosophila* oogenesis have been studied extensively. However, as illustrated by this study and ref. 49, additional unsuspected roles for E-Cad remain to be identified. One of the reasons these roles have not been identified previously is that, as shown in *Drosophila* follicular epithelium (40), in mammals (52, 53), and, as we report, in GCs, N-Cad compensates for E-Cad function. Our observations also provide a rationale for the previous discrepancy between E-Cad (no multinucleation) and β-Cat (multinucleation) phenotypes in the GCs (6, 38). We further propose that similar functional intercompensation between classical cadherins is likely to occur in a number of other tissues, developmental stages, and organisms and is likely to bias observations similarly, depending on the methods used to affect E-Cad function.

AP-1/Rab11/E-Cad are required for maintenance of RCs' attachment throughout vitellogenesis, during which faster cellular growth is accompanied by an increase in PM tension. We therefore propose that RCs' anchoring must be reinforced through the AP-1–mediated delivery of E-Cad to withstand the increased membrane tension generated by exponential growth during vitellogenesis. Without reinforcement, these forces would be sufficient to tear the PM surrounding the RCs physically. Why would the PM tear only at this location and not anywhere else? We can only suppose that dynamic rearrangements of the PM surrounding RCs that are required either to organize the microvilli-rich region or to accommodate the growth of RCs somehow destabilize the PM. Based on the conservation of the RC functions in the germlines of invertebrates and vertebrates, we anticipate that this function of E-Cad is evolutionarily conserved.

Materials and Methods

Materials and methods are briefly described here. Further details are given in *SI Materials and Methods*.

***Drosophila* Stocks and Genetics.** *AP-47*^{SHE11}, *shg*^{R69}, and *arm*^{XP33} mutant germline clones were generated using the FLP/FRT system. The MTD-GAL4 line was used to drive RNAi and Rab11 dominant-negative expression in the germ line.

Immunofluorescence and Antibodies. Ovaries from adult flies were fixed in 4% (wt/vol) paraformaldehyde and stained with primary antibodies: rat anti–DE-Cad [1:100; DCAD2; Developmental Studies Hybridoma Bank (DSHB)], rat anti–N-Cad (1:500; DSHB), mouse anti-Rab11 (1:100; DSHB), mouse anti-Armadillo (1:200; N27A1; DSHB), rabbit anti–γ-Adaptin (1:1,000) (54), rat anti–α-Actn (1:50; DSHB), mouse anti–Hts-RC (1:5; Creative Diagnostics), and rabbit anti–P-Moesin (1:100) (55). We then used Cy2-, Cy3-, or Cy5-coupled secondary antibodies (Jackson Laboratories) diluted 1:250 and/or Phalloidin–Alexa-647 (Life Technology) diluted 1:500.

Imaging and Laser Ablation. Live ovarioles were dissected and maintained in Schneider medium adjusted to pH 7.0 after supplementation with 15% (vol/vol) FCS and 200 μg/mL bovine insulin, as described in ref. 56. Fixed specimens and movies were acquired using LSM Leica SP5 and SP8 microscopes equipped with a 63× plan Apo-NA 1.4 lens or using a spinning-disk confocal microscopy equipped with a CSU-X1 disk, a Cool-SNAP-HQ2 camera, a Piezo stage, and a 100/3 plan Apo-NA 1.4 lens under the control of the MetaMorph Software. All images were processed using ImageJ.

Laser ablation was performed on live GCs using a Leica SP5 confocal microscope. Ablation was carried out on nurse cell membranes 16.5 ± 0.5 μm below the coverslip with a two-photon laser-type Mai-Tai HP from Spectra Physics set to 800 nm.

EM. Ovaries were fixed in 2% (wt/vol) paraformaldehyde plus 2.5% (wt/vol) glutaraldehyde in 0.1 M cacodylate buffer for 2 h at room temperature and were processed for uranyl acetate contrast and embedded in Epon-Araldite mix (57, 58). Samples were observed directly either after ultrathin sectioning using a JEOL JEM-1400 electron microscope (Jeol) operated at 80 kV, equipped with a Gatan ORIUS SC1000 camera, or with a Gatan 3View microtome within an FEI Quanta 250 field emission gun scanning electron microscope as described in ref. 57.

ACKNOWLEDGMENTS. We thank F. Payre, A. Guichet, Y. Hong, U. Tepass, the Bloomington and Kyoto *Drosophila* stock centers, the Drosophila Transgenic RNAi Project at Harvard Medical School (NIH/National Institute of General Medical Sciences), and the Developmental Studies Hybridoma Bank (Iowa); A. Guichet and N. Tissot (Institut Jacques Monod) for teaching N.L. to perform time-lapse imaging of GCs; T. Starborg from the EM facility in the

Faculty of Life Sciences for their assistance, and the Wellcome Trust for equipment grant support to the EM facility; the Microscopy Rennes Imaging Center; and A. Guichet, S. Le Bras, J. Mathieu, A. Pacquelet, and P. Thérond for critical reading of the manuscript. This work was funded by the CNRS, Ligue Nationale Contre le Cancer, and Agence Nationale pour la Recherche. N.L. received doctoral fellowships from the Ministère Nationale pour l'Education, la Recherche et la Technologie and Association pour la Recherche sur le Cancer.

1. Le TL, Yap AS, Stow JL (1999) Recycling of E-cadherin: A potential mechanism for regulating cadherin dynamics. *J Cell Biol* 146(1):219–232.
2. Classen AK, Anderson KI, Marois E, Eaton S (2005) Hexagonal packing of Drosophila wing epithelial cells by the planar cell polarity pathway. *Dev Cell* 9(6):805–817.
3. Harris KP, Tepass U (2008) Cdc42 and Par proteins stabilize dynamic adherens junctions in the Drosophila neuroectoderm through regulation of apical endocytosis. *J Cell Biol* 183(6):1129–1143.
4. Shaye DD, Casanova J, Llimargas M (2008) Modulation of intracellular trafficking regulates cell intercalation in the Drosophila trachea. *Nat Cell Biol* 10(8):964–970.
5. Levayer R, Pelissier-Monier A, Lecuit T (2011) Spatial regulation of Dia and Myosin-II by RhoGEF2 controls initiation of E-cadherin endocytosis during epithelial morphogenesis. *Nat Cell Biol* 13(5):529–540.
6. Oda H, Uemura T, Takeichi M (1997) Phenotypic analysis of null mutants for DE-cadherin and Armadillo in Drosophila ovaries reveals distinct aspects of their functions in cell adhesion and cytoskeletal organization. Genes Cells 2(1):29–40.
7. Niewiadomska P, Godt D, Tepass U (1999) DE-Cadherin is required for intercellular motility during Drosophila oogenesis. *J Cell Biol* 144(3):533–547.
8. Song X, Zhu CH, Doan C, Xie T (2002) Germline stem cells anchored by adherens junctions in the Drosophila ovary niches. *Science* 296(5574):1855–1857.
9. Haglund K, Nezis IP, Stenmark H (2011) Structure and functions of stable intercellular bridges formed by incomplete cytokinesis during development. *Commun Integr Biol* 4(1):1–9.
10. McLean PF, Cooley L (2013) Protein equilibration through somatic ring canals in Drosophila. *Science* 340(6139):1445–1447.
11. Warn RM, Gutzeit HO, Smith L, Warn A (1985) F-actin rings are associated with the ring canals of the Drosophila egg chamber. *Exp Cell Res* 157(2):355–363.
12. Mahowald AP (1971) The formation of ring canals by cell furrows in Drosophila. *Z Zellforsch Mikrosk Anat* 118(2):162–167.
13. Robinson DN, Cant K, Cooley L (1994) Morphogenesis of Drosophila ovarian ring canals. *Development* 120(7):2015–2025.
14. Kelso RJ, Hudson AM, Cooley L (2002) Drosophila Kelch regulates actin organization via Src64-dependent tyrosine phosphorylation. *J Cell Biol* 156(4):703–713.
15. Yue L, Spradling AC (1992) hu-li tai shao, a gene required for ring canal formation during Drosophila oogenesis, encodes a homolog of adducin. *Genes Dev* 6(12B): 2443–2454.
16. Sokol NS, Cooley L (1999) Drosophila filamin encoded by the cheerio locus is a component of ovarian ring canals. *Curr Biol* 9(21):1221–1230.
17. Field CM, Alberts BM (1995) Anillin, a contractile ring protein that cycles from the nucleus to the cell cortex. *J Cell Biol* 131(1):165–178.
18. Coutelis JB, Ephrussi A (2007) Rab6 mediates membrane organization and determinant localization during Drosophila oogenesis. *Development* 134(7):1419–1430.
19. Vaccari T, et al. (2009) Comparative analysis of ESCRT-I, ESCRT-II and ESCRT-III function in Drosophila by efficient isolation of ESCRT mutants. *J Cell Sci* 122(Pt 14):2413–2423.
20. Murthy M, et al. (2005) Sec6 mutations and the Drosophila exocyst complex. *J Cell Sci* 118(Pt 6):1139–1150.
21. Murthy M, Schwarz TL (2004) The exocyst component Sec5 is required for membrane traffic and polarity in the Drosophila ovary. *Development* 131(2):377–388.
22. Januschke J, et al. (2007) Rab6 and the secretory pathway affect oocyte polarity in Drosophila. *Development* 134(19):3419–3425.
23. Tan J, Oh K, Burgess J, Hipfner DR, Brill JA (2014) PI4KIIIα is required for cortical integrity and cell polarity during Drosophila oogenesis. *J Cell Sci* 127(Pt 5):954–966.
24. Bogard N, Lan L, Xu J, Cohen RS (2007) Rab11 maintains connections between germline stem cells and niche cells in the Drosophila ovary. *Development* 134(19): 3413–3418.
25. Bonifacino JS (2014) Adaptor proteins involved in polarized sorting. *J Cell Biol* 204(1): 7–17.
26. Nicolas E, Chenouard N, Olivo-Marin JC, Guichet A (2009) A dual role for actin and microtubule cytoskeleton in the transport of Golgi units from the nurse cells to the oocyte across ring canals. *Mol Biol Cell* 20(1):556–568.
27. Römer W, et al. (2007) Shiga toxin induces tubular membrane invaginations for its uptake into cells. *Nature* 450(7170):670–675.
28. Manneville JB, et al. (2008) COPI coat assembly occurs on liquid-disordered domains and the associated membrane deformations are limited by membrane tension. *Proc Natl Acad Sci USA* 105(44):16946–16951.
29. Diz-Muñoz A, Fletcher DA, Weiner OD (2013) Use the force: Membrane tension as an organizer of cell shape and motility. *Trends Cell Biol* 23(2):47–53.
30. Huang J, Zhou W, Dong W, Watson AM, Hong Y (2009) From the Cover: Directed, efficient, and versatile modifications of the Drosophila genome by genomic engineering. *Proc Natl Acad Sci USA* 106(20):8284–8289.
31. Delevoye C, et al. (2009) AP-1 and KIF13A coordinate endosomal sorting and positioning during melanosome biogenesis. *J Cell Biol* 187(2):247–264.
32. Schmidt MR, et al. (2009) Regulation of endosomal membrane traffic by a Gadkin/AP-1/kinesin KIF5 complex. *Proc Natl Acad Sci USA* 106(36):15344–15349.
33. Lock JG, Stow JL (2005) Rab11 in recycling endosomes regulates the sorting and basolateral transport of E-cadherin. *Mol Biol Cell* 16(4):1744–1755.
34. Ling K, et al. (2007) Type I gamma phosphatidylinositol phosphate kinase modulates adherens junction and E-cadherin trafficking via a direct interaction with mu 1B adaptin. *J Cell Biol* 176(3):343–353.
35. Desclozeaux M, et al. (2008) Active Rab11 and functional recycling endosome are required for E-cadherin trafficking and lumen formation during epithelial morphogenesis. *Am J Physiol Cell Physiol* 295(2):C545–C556.
36. Ren M, et al. (1998) Hydrolysis of GTP on rab11 is required for the direct delivery of transferrin from the pericentriolar recycling compartment to the cell surface but not from sorting endosomes. *Proc Natl Acad Sci USA* 95(11):6187–6192.
37. White P, Aberle H, Vincent JP (1998) Signaling and adhesion activities of mammalian beta-catenin and plakoglobin in Drosophila. *J Cell Biol* 140(1):183–195.
38. Peifer M, Orsulic S, Sweeton D, Wieschaus E (1993) A role for the Drosophila segment polarity gene armadillo in cell adhesion and cytoskeletal integrity during oogenesis. *Development* 118(4):1191–1207.
39. Godt D, Tepass U (1998) Drosophila oocyte localization is mediated by differential cadherin-based adhesion. *Nature* 395(6700):387–391.
40. Grammont M (2007) Adherens junction remodeling by the Notch pathway in Drosophila melanogaster oogenesis. *J Cell Biol* 177(1):139–150.
41. Denk W, Horstmann H (2004) Serial block-face scanning electron microscopy to reconstruct three-dimensional tissue nanostructure. *PLoS Biol* 2(11):e329.
42. Wahlström G, Lahti VP, Pispa J, Roos C, Heino TI (2004) Drosophila non-muscle alpha-actinin is localized in nurse cell actin bundles and ring canals, but is not required for fertility. *Mech Dev* 121(11):1377–1391.
43. Gates J, et al. (2009) Enabled and Capping protein play important roles in shaping cell behavior during Drosophila oogenesis. *Dev Biol* 333(1):90–107.
44. Hase K, et al. (2013) *1B*-mediated protein sorting regulates polarity and proliferation of intestinal epithelial cells in mice. *Gastroenterology* 145(3):625–635.
45. Gillard G, et al. (2015) Control of E-cadherin apical localisation and morphogenesis by a SOAP-1/AP-1/clathrin pathway in C. elegans epidermal cells. *Development* 142(9): 1684–1694.
46. Langevin J, et al. (2005) Drosophila exocyst components Sec5, Sec6, and Sec15 regulate DE-Cadherin trafficking from recycling endosomes to the plasma membrane. *Dev Cell* 9(3):365–376.
47. Tong C, et al. (2011) Rich regulates target specificity of photoreceptor cells and N-cadherin trafficking in the Drosophila visual system via Rab6. *Neuron* 71(3):447–459.
48. Schlichting K, Wilsch-Bräuninger M, Demontis F, Dahmann C (2006) Cadherin Cad99C is required for normal microvilli morphology in Drosophila follicle cells. *J Cell Sci* 119(Pt 6):1184–1195.
49. Crawley SW, et al. (2014) Intestinal brush border assembly driven by protocadherin-based intermicrovillar adhesion. *Cell* 157(2):433–446.
50. Glowinski C, Liu RH, Chen X, Darabie A, Godt D (2014) Myosin VIIA regulates microvillus morphogenesis and interacts with cadherin Cad99C in Drosophila oogenesis. *J Cell Sci* 127(22):4821–4832.
51. Huelsmann S, Ylänne J, Brown NH (2013) Filopodia-like actin cables position nuclei in association with perinuclear actin in Drosophila nurse cells. *Dev Cell* 26(6):604–615.
52. Kuphal S, Poser I, Jobin C, Hellerbrand C, Bosserhoff AK (2004) Loss of E-cadherin leads to upregulation of NFkappaB activity in malignant melanoma. *Oncogene* 23(52):8509–8519.
53. Hawkins K, Mohamet L, Ritson S, Merry CL, Ward CM (2012) E-cadherin and, in its absence, N-cadherin promotes Nanog expression in mouse embryonic stem cells via STAT3 phosphorylation. *Stem Cells* 30(9):1842–1851.
54. Benhra N, et al. (2011) AP-1 controls the trafficking of Notch and Sanpodo toward E-cadherin junctions in sensory organ precursors. *Curr Biol* 21(1):87–95.
55. Polesello C, Delon I, Valenti P, Ferrer P, Payre F (2002) Dmoesin controls actin-based cell shape and polarity during Drosophila melanogaster oogenesis. *Nat Cell Biol* 4(10): 782–789.
56. Prasad M, Jang AC, Starz-Gaiano M, Melani M, Montell DJ (2007) A protocol for culturing Drosophila melanogaster stage 9 egg chambers for live imaging. *Nat Protoc* 2(10):2467–2473.
57. Starborg T, et al. (2013) Using transmission electron microscopy and 3View to determine collagen fibril size and three-dimensional organization. *Nat Protoc* 8(7): 1433–1448.
58. Kolotuev I (2014) Positional correlative anatomy of invertebrate model organisms increases efficiency of TEM data production. *Microsc Microanal* 20(5):1392–1403.
59. Claret S, Jouette J, Benoit B, Legent K, Guichet A (2014) PI(4,5)P2 produced by the PI4P5K SKTL controls apical size by tethering PAR-3 in Drosophila epithelial cells. *Curr Biol* 24(10):1071–1079.
60. King RC (1970) *Ovarian Development in Drosophila melanogaster* (Academic, New York).
61. Hayashi K, Yonemura S, Matsui T, Tsukita S (1999) Immunofluorescence detection of ezrin/radixin/moesin (ERM) proteins with their carboxyl-terminal threonine phosphorylated in cultured cells and tissues. *J Cell Sci* 112(Pt 8):1149–1158.